

Title

Assessment of low-temperature degradation of Y-TZP ceramics based on Raman-spectroscopic analysis and hardness indentation

Authors

Schröder, C.*; Renz, A.; Koplin, C.; Kailer, A.

Fraunhofer Institute for Mechanics of Materials IWM, Business Unit Tribology, Freiburg, Germany

0 Abstract

This paper focuses on the analysis of hydrothermally induced phase transformation of yttria-stabilized tetragonal polycrystalline zirconia (Y-TZP) and its influence on the hardness. Due to the hydrothermal exposure and the accompanied low temperature degradation (LTD), a micro-cracked transformation zone is generated at the surface and progresses into the subjacent material. Raman-spectroscopic analysis of hydrothermally loaded and cross-sectioned samples revealed complete phase transformation within this zone. Its depth as well as its temperature-dependent growth rate was verified. Raman-spectroscopic measurements at the surfaces were correlated with the progression of the transformation zone. An efficient model, which assumes one extinction coefficient for tetragonal and monoclinic microstructure, enables to determine the depth of the transformation zone from the measured Raman signals. Furthermore, an exponentially decreasing Vickers hardness with increasing depth was determined. Finally, a differently sintered Y-TZP ceramic revealed enhanced resistance against LTD for the same hydrothermal loading conditions.

1 Introduction

Yttria-stabilized tetragonal zirconia polycrystalline (Y-TZP) ceramics are promising materials for many technical applications as they provide a very high hardness and fracture toughness and mechanical strength [1] [2] [3] [4]. Furthermore, due to their corrosion and wear resistance and biocompatibility, they are utilized for artificial femoral heads and dental restorations [1] [5]. The reliability of some zirconia ceramics is still limited by undesired phase transformation in contact with aqueous solutions which is known as “Low Temperature Degradation” (LTD). This degradation is characterized by nucleation and growth of a transformed and destabilized zone from the hydrothermally loaded surface into the bulk material [6]. Due to the accompanied intergranular micro-cracking, LTD causes a loss of mechanical strength [7]. Extensive research on LTD of zirconia ceramics has been done in recent

years [6] [8]. In this context, research mainly focused on microstructural features, which affect the resistance to degradation. The addition of alumina to zirconia is for instance a suitable method to decelerate the aging process [9]. Further promising approaches are the decrease of both, the grain size and tensile residual stresses within the material [6]. An excellent review was published by Basu [2], which generally summarizes different microstructural features that have an impact on the phase transformation. In addition, Chevalier [6] investigated the characteristic features of LTD. In summary, it can be stated that the production of aging-resistant zirconia ceramics requires an accurate setting of relevant process stages like powder mixing, sintering and machining.

In general, the experimental examination of LTD is carried out using hydrothermal ageing experiments. Subsequent investigations enable the quantification of the ratio of tetragonal and transformed monoclinic phases. Here, μ -Raman-spectroscopy has become a widely used method as it is very sensitive to monoclinic zirconia and offers a high spatial resolution [10] [11].

Based on previous research, mathematical correlations were identified between the transformed monoclinic phase content V_m and both the absolute hydrothermal loading temperature T and time of exposure to moisture t . On the basis of surface analysis it was concluded that the transformation kinetics follow the Mehl-Avrami-Johnson (MAJ) law as depicted in Equation 1 [10] [12]:

$$V_m = 1 - e^{-(b \cdot t)^n} \quad \text{Equation 1}$$

where the Avrami-exponent n depends on the nucleation-and-growth kinetics of the aging process with typical values between 0,3 and 3,5 [13]. The reaction rate constant b corresponds to the Arrhenius law in Equation 2:

$$b = b_0 \cdot e^{\frac{-Q}{R \cdot T}} \quad \text{Equation 2}$$

where R is the gas constant and b_0 is a constant pre-exponential factor that refers to the reaction mechanism of the transformation process. Q is the activation energy of the tetragonal to monoclinic transformation, which depends on both temperature and microstructure [14].

Nevertheless, conclusions about the actually existing phase contents from Raman-spectroscopic measurements have to be drawn carefully. In fact, the detected Raman-signals originate not only from the surface of zirconia samples but from subsurface areas as well. In that regard, Presser et al. [15] state that the information depth in a Raman analysis depends on material and instrumental parameters as well as the microscope setup and may therefore extend “to several tens of μm ” [15] for a non-degraded Y-TZP ceramic.

In order to determine phase transformation beneath the surface, Muñoz-Tabares et al. [7] experimentally investigated cross sections of hydrothermally loaded zirconia ceramics. While a high value of the monoclinic content was detected close to the surface, a steep gradient was observed at a certain depth where the monoclinic phase content dropped to almost zero. The gradual change from the saturated value of monoclinic phase to untransformed tetragonal structure occurs within a short distance of about $15\ \mu\text{m}$. This observation leads to the assumption that hydrothermally loaded ceramics may consist of a highly transformed zone with high monoclinic phase content and sharp transition to the untransformed bulk. Further investigations by Keuper et al. [16] using SEM/EBSD techniques yielded evidence that the transformation front is rather sharp.

As Raman signals are obtained from certain depths in the material and the surface-near areas of hydrothermally loaded samples are expected to be completely transformed, Raman-spectroscopic measurements on the surfaces can be illustrated as depicted in Fig. 1.

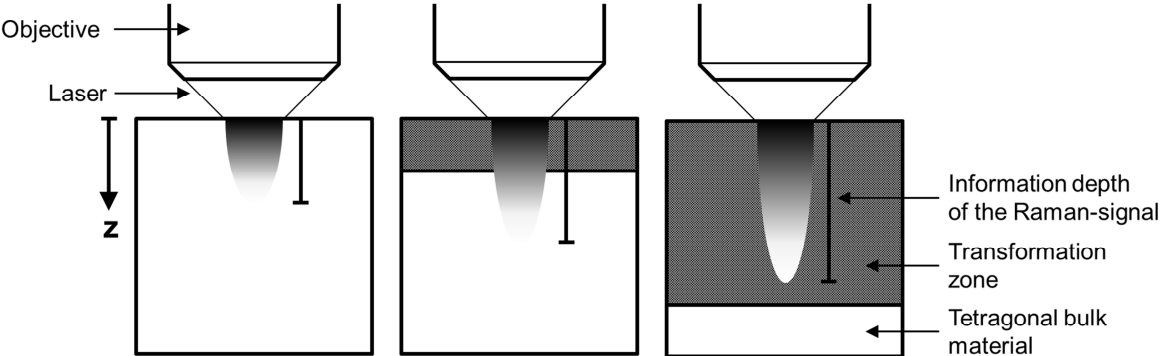


Fig. 1: Raman-signals are detected in the bulk material as well as in the transformed zone for hydrothermally loaded samples. It is expected that the information depths change due to the different absorption coefficients and thicknesses of the zones.

For a small transformation depth it is clear that a considerable part of the measured Raman intensity is detected from non-transformed subsurface areas. As the transformation front progresses into the bulk material as a consequence of further degradation, the ratio of transformed monoclinic zirconia within the Raman-probe volume increases. Taking this circumstance into account, it becomes clear that for an accurate characterization of the growth behavior of the transformation zone careful interpretation of the Raman-data is necessary. Only with this knowledge of depth-dependent signal response, Raman-spectroscopic measurements on the surfaces can be interpreted correctly and used to reliably determine the depth of the transformation zone without further sample preparations.

The objective of this work was to quantify and compare the phase transformation rates of two differently processed Y-TZP ceramics after defined hydrothermal loading conditions. Therefore, the size of transformation zones and their microstructures were characterized via optical microscopy and SEM after cross-sectioning of the degraded samples. Raman-spectroscopy was applied on the surfaces after hydrothermal loading as well as within the bulk material of cross-sectioned samples. Moreover, the materials' macro hardness was investigated via Vickers indentation in order to examine the impact of hydrothermal loading on the mechanical response. The results of these three investigations were correlated to describe the impact of LTD on the material.

2 Material and methods

Two differently sintered high strength zirconia ceramics (3 mol.% yttria, 0,2-0,3 wt. % alumina, FCT Hartbearbeitungs GmbH, Sonneberg, Germany) were investigated: On the one hand Y-TZP standard material exhibiting a grain size of 0,4 μm and on the other HY-TZP with an average grain size of 0,28 μm . The "H" refers to a modified sintering process, including an additional hot isostatic pressing step.

The experiments were conducted on rectangular bending bar samples with dimensions of 3 mm x 4 mm x 20 mm. The 4 mm x 20 mm faces of the bending bars were polished to ensure accurate Vickers indentations according to industrial standards [17]. Polishing was carried out as a multistage process with gradually different fine-grained diamond suspensions for various times in order to minimize preparation damages. The particular preparation steps are depicted in Table 1.

Table 1: Steps of the polishing process for the sample surfaces/cross-section preparation.

| | Diamond suspension | Time |
|---|----------------------------|--------|
| Surface machining / Cross-sectioning | 30 μm | 20 min |
| | 9 μm | 10 min |
| | 3 μm | 15 min |
| | 1 μm | 5 min |
| | Oxide polishing suspension | 4 min |

The ceramic samples were hydrothermally aged in a saturated water steam atmosphere by using an autoclave system (Autoclave DD 050 SS 33, Autoclave Engineers, Erie, USA) under consideration of certain loading temperatures, pressures and times as arising from Table 2.

Table 2: Hydrothermal loading conditions for certain aging processes of Y-TZP and HY-TZP ceramics. HY-TZP was not included in series A since no change was observed in series B.

| Experimental series | Temperature | Pressure | Time |
|---------------------|-------------|----------|------|
| A | 175 °C | 9 bar | 4 h |
| | | | 8 h |
| | | | 16 h |
| | | | 24 h |
| B | 200 °C | 15,5 bar | 2 h |
| | | | 4 h |
| | | | 8 h |
| | | | 16 h |
| | | | 24 h |
| C | 225 °C | 26 bar | 2 h |
| | | | 4 h |
| | | | 8 h |

Raman microscopy (InVia, Renishaw, Gloucestershire, UK) was applied using a Nd:YAG (SHG) laser with a wavelength of 532 nm. As the tetragonal and monoclinic phases give rise to specific Raman bands respectively, the phase fractions can be derived by setting the integrated intensities of the characteristic Raman bands for the tetragonal (I_t^{147} , I_t^{265}) and monoclinic (I_m^{181} , I_m^{190}) phase in relation to each other as in Equation 3 which was introduced by Clarke et al. [18].

$$V_m = \frac{I_m^{181} + I_m^{190}}{k \cdot (I_t^{147} + \delta \cdot I_t^{265}) + I_m^{181} + I_m^{190}} \quad \text{Equation 3}$$

k and δ are empirical factors with values of $k = 0,97$ and $\delta = 1$ [18]. The super-indexes of the integrated intensities refer to the positions of the Raman bands. Due to the uncertainties related to superficial Raman-spectroscopic measurements as mentioned above, the calculated results will not be interpreted as monoclinic contents. In fact, they just represent intensity ratios. The intensities were calculated on the basis of a curve fitting procedure (WIRE 3.4 software, Renishaw, Gloucestershire, UK) according to Dorn [19] [20].

Hydrothermally aged samples were cut using a diamond band saw. The resulting cross-sections were embedded in polyester resin and machined according to the preparation steps listed in Table 1. The subsurface transformation zone was investigated using digital (VHX 500 F, Keyence Deutschland GmbH, Neu-Isenburg, Germany) and scanning electron microscopy (Zeiss Supra 55VP, Carl Zeiss AG, Oberkochen, Germany) as well as Raman-spectroscopy.

In order to measure the materials' macro-hardness after hydrothermal loading, 5 Vickers indentations (Dia Testor 2 RC, Otto Wolpert-Werk GmbH, Ludwigshafen, Germany) were made on the polished surfaces of each sample using a loading force of 50 N. Additionally, 19 nanoindentations (Fischerscope H100C, Helmut Fischer GmbH, Sindelfingen, Germany) were applied at both, the transformation zone and subjacent tetragonal structure of the polished surfaces of a cross-section. One Y-TZP sample, which was hydrothermally loaded at $T = 200$ °C for $t = 16$ h was used for these investigations. The indentations within the transformation zone were set at least at distances of 75 μm from the surface respectively the transformation front. From the measured indentation depths h_c and h_{max} the averaged material's hardness H , stiffness S and effective Young's modulus E_{eff} were determined using the method of Oliver and Pharr [21] [22] (Equations 4-8). Vickers indentations were carried out using a loading force of 500 mN and a loading rate of 500 mN/60 s.

$$H = \frac{P_{max}}{A(h_c)} \quad \text{Equation 4}$$

$$S = \varepsilon \cdot \frac{P_{max}}{h_s} \quad \text{Equation 5}$$

$$E_{eff} = \frac{1}{\beta} \cdot \frac{\sqrt{\pi}}{2} \cdot \frac{S}{\sqrt{A(h_c)}} \quad \text{Equation 6}$$

$$A(h_c) = 24,561 \cdot (h_c + 0,008)^2 + 0,206 \cdot (h_c + 0,008) \quad \text{Equation 7}$$

$$h_s = h_{max} - h_c \quad \text{Equation 8}$$

with $\beta = 1,05$ [23] and $\varepsilon = 0,75$ [21] [22].

3 Results

In order to visualize the changed microstructural features due to hydrothermal loading, Fig. 2 shows typical cross sections of aged samples that exhibit a clearly visible transformation zone.

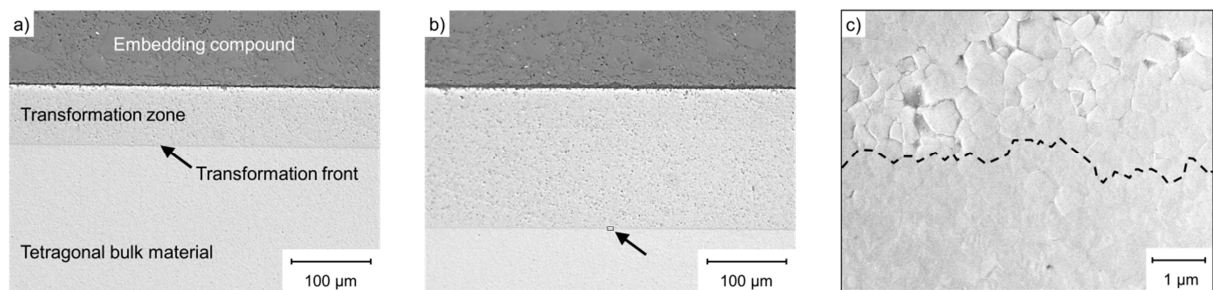


Fig. 2: Digital (a) and b)) and SE microscope images (c)) of differently aged Y-TZP ceramics after cross-sectioning; a): $T = 175 \text{ }^\circ\text{C}$, $t = 24 \text{ h}$; b) and c): $T = 225 \text{ }^\circ\text{C}$, $t = 4 \text{ h}$. The dashed line in the enlarged view of c) refers to the transformation front.

The transformation zone and the non-degraded bulk material can be distinguished by digital microscopy due to different light reflections of these areas. A sharp transition line expands parallel to the surface and therefore enables to precisely measure the depth of the transformation zone. Moreover, the comparison between Fig. 2a) and b) shows the changed progression of the transformation front into the bulk material due to changed hydrothermal loading conditions. Intergranular disruption is visible via SEM as shown in the enlarged view in Fig. 2c). The detail view on the transformation front reveals the sharp transition between the micro-cracked and undamaged zones. The grain pull-out in the transformation zone is assumed to result from the surficial machining procedure, as the interconnections between the grains are significantly weakened.

Fig. 3 illustrates the phase transformation behavior within the bulk material by exemplarily analyzing the cross-sectioned samples of the experimental series B nearby the transformation fronts.

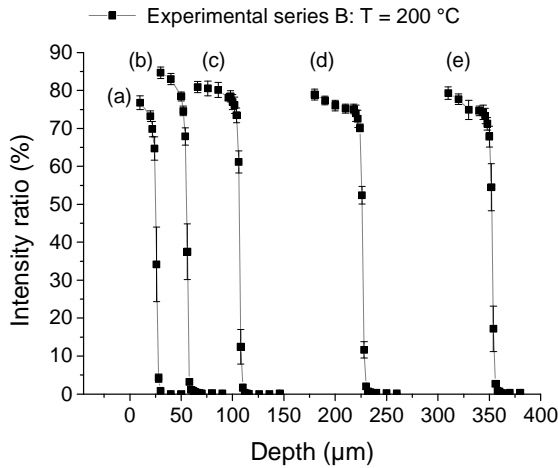


Fig. 3: Intensity ratios measured nearby the microscopically observed transformation fronts after hydrothermal loading of Y-TZP ceramics for 200 °C and various times: a) 2 h, b) 4 h, c) 8 h, d) 16 h and e).

The curves are characterized by a sharp decrease of the intensity ratios at certain depths from the surfaces. These depths match very well with the microscopically observed depths of the transformation fronts as drawn in Fig. 4. The very high intensity ratios of ca. 80 % give evidence about the full transformation within the transformed zones.

The depth values of the transformation zones are plotted as function of hydrothermal exposure duration and temperatures in Fig. 4 for all experimental series.

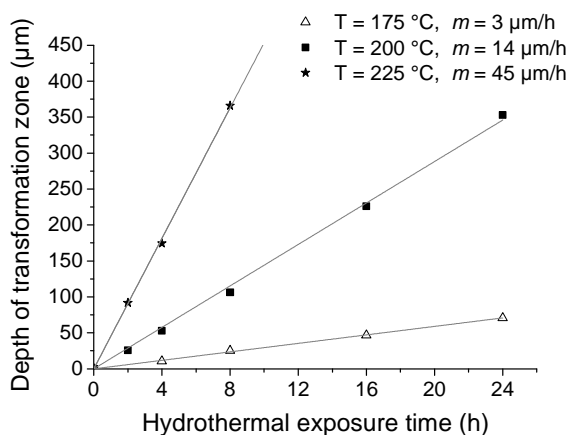


Fig. 4: Depths of the transformation zones within the bulk materials of Y-TZP ceramics related to various hydrothermal loading times and temperatures.

The diagram shows well correlating linear relationships for each temperature. It can be seen, that the slopes m of the linear trendlines increase considerably with increasing temperature.

Fig. 5 shows the time- and temperature-dependent progression of the Raman-band intensity ratios determined on hydrothermally loaded sample surfaces. The relations between intensity ratios and loading times are illustrated as solid lines and follow a modified MAJ law (Equation 9) considering a saturated intensity ratio of 80 % and a constant Avrami-exponent $n = 1$.

$$V_m = 80 \% \cdot (1 - e^{-b \cdot t}) \quad \text{Equation 9}$$

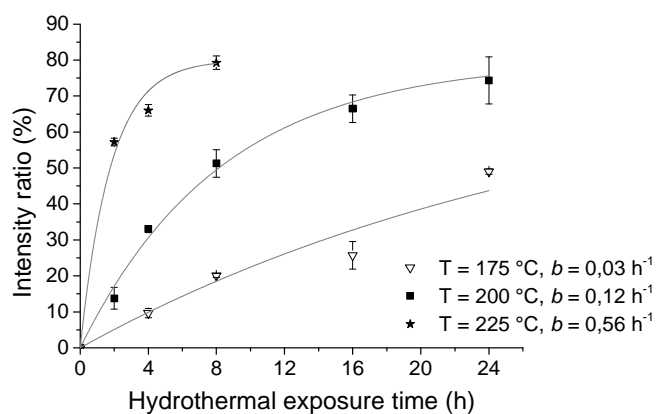


Fig. 5: Intensity ratios determined via Raman-Spectroscopy on the surfaces of various hydrothermally loaded Y-TZP samples. The solid lines correspond to a computational fitting procedure with $n = 1$.

The correlation of these two completely different descriptions of phase transformation behavior, on the one hand the transformation zone depths determined via light microscopy and on the other hand the Raman-spectroscopic investigations on the surfaces, leads to Fig. 6.

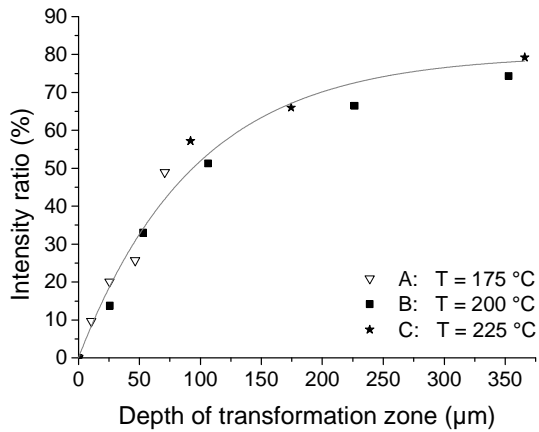


Fig. 6: Intensity ratios determined via Raman-spectroscopy on the surfaces related to the depths of the transformation zone of various hydrothermally loaded Y-TZP samples.

The measured intensity ratios of all investigated experimental series progress with increasing depth of the transformation zone, following one exponential law. The specific hydrothermal loading conditions, like exposure time and temperature, do therefore not directly influence the intensity ratio, as there is only a correlation to the depth of transformation zone.

Another correlation, which depends only on the depth of the transformation zone, is the changed macro-hardness of Y-TZP due to hydrothermal loading as displayed in Fig. 7.

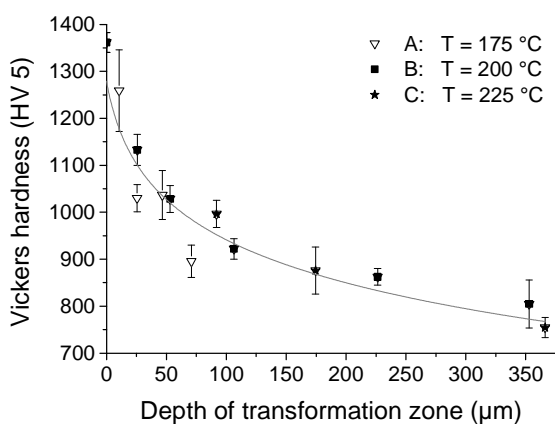


Fig. 7: Measured Vickers hardness of Y-TZP ceramics related to the depths of the transformation zones.

It can be seen that the Vickers hardness exponentially decreases with increasing depth.

The values for hardness, stiffness and effective Young's modulus which were determined on the basis of nanoindentation tests at the polished surface of a cross-section are listed in Table 3. Additionally, the averaged loading and unloading curves are illustrated in Fig. 8. Steady curve progressions could be observed for all applied nanoindentations within the tetragonal bulk material as well as the transformation zone.

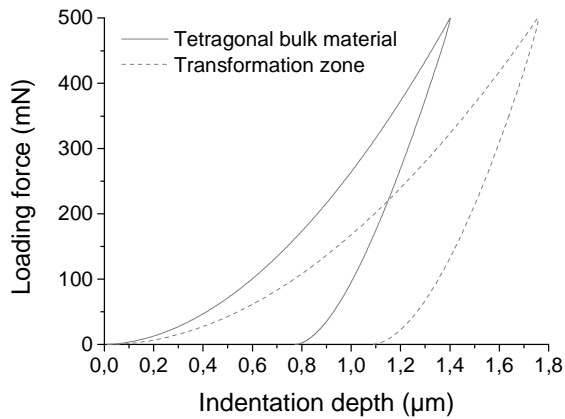


Fig. 8: Averaged loading and unloading curves of the nanoindentation tests within the cross-section of a hydrothermally loaded Y-TZP ceramic.

Table 3: Values for hardness, stiffness and effective Young's modulus on the basis of nanoindentation tests at the polished surface of a cross-section.

| | Hardness HV 0,5 | Hardness H | Stiffness S | Effective Young's modulus E_{eff} |
|-----------------------------|-----------------|--------------|------------------|-------------------------------------|
| Transformation zone | 872 | 9,3 GPa | 1286 mN/ μ m | 148,3 GPa |
| Tetragonal structure | 1535 | 16,4 GPa | 1262 mN/ μ m | 192,6 GPa |

While hardness and effective Young's modulus of the transformation zone are lower compared to the tetragonal structure, the material's stiffness is almost the same in both cases.

In contrast to the results above, the hot isostatically pressed HY-TZP shows a completely different phase transformation behavior. Neither any indication of a growing transformation zone at cross-sections nor local phase transformations at the surface were detected via Raman-spectroscopy or within the bulk material after applying various hydrothermal loading condition.

The hardness values of the HY-TZP have not been affected by hydrothermal exposure, as the same macro hardness value of 1390 HV5 was measured for all investigated HY-TZP samples.

4 Discussion

Raman-spectroscopic analysis of cross-sectional cuts through the hydrothermally degraded specimens reveal a sharp boundary between the completely transformed zone and the tetragonal bulk material, i.e. no transition zone with mixed phases could be identified.

The depth of the transformation zone and the hydrothermal exposure time show a strong correlation that allows a reliable prediction of the depth for specific hydrothermal conditions. As derived from the linear progression of the transformation zone (Fig. 4), the slope *m* can be interpreted as the rate of growth of the transformation zone. As the slopes are constant for distinct temperatures over the whole measuring range, it is confirmed that the rate of growth is independent of depth, but only from time and temperature. This behavior refers to an autocatalytic process, which is generated by water intruding into the material to the transformation front via micro-cracks and there continuously activates phase transformation [6]. The rate of growth found by Keuper et al. amounts to 0,0624 μm/h at a temperature of 134°C [16]. As the materials' composition, density and grain size range of their Y-TZP ceramic is comparable with the material from the present work, this value is additionally shown in Fig. 9.

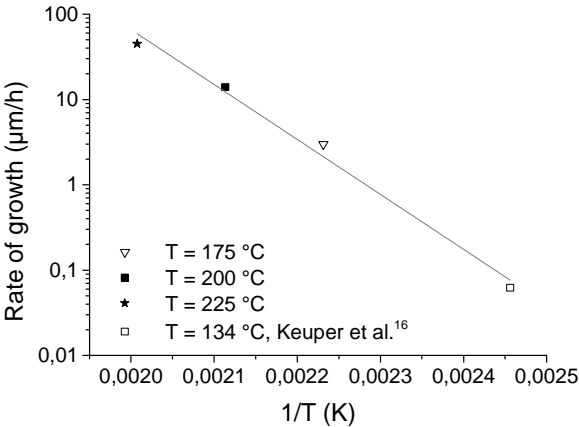


Fig. 9: Examined rates of growth of the transformation zones related to the inverse hydrothermal loading temperatures.

From these results, it is possible to approximate the growth rate of the transformation zone within the temperature range from 134 °C to 225 °C. Thus, the duration until a specific degree of transformation is reached, that causes a change of mechanical properties, is determinable.

As in previous publications, the phase transformation behavior was determined from Raman-spectroscopic measurements on the surfaces of hydrothermally loaded Y-TZP samples. It was shown there that the increase of the intensity ratio with time and temperature follows the MAJ law [24] [7]. Assuming a constant value of n for the investigated temperatures is feasible, as the results in Fig. 4 indicate that the transformation mechanism does not change time-dependently. In fact, the linear curves reveal the continuously stable progression of phase transformation, which is expected to proceed unsteadily due to changed transformation kinetics.

The transformation zone depth shows a well-fitting exponential correlation with the measured intensity ratio on the surface as drawn in Fig. 6. The high stability index of the fitted curve furthermore indicates a good reproducibility of the results in the above mentioned experimental setup. Given that Raman-spectroscopic measurements do not represent the actual state of monoclinic phases on the surface, it was shown that the gathered intensity ratios are still useful to estimate the depths of transformation zones. From the results it can be summarized, that especially for low hydrothermal loading conditions, a slight progression of the transformation zone has a strong impact on the calculated intensity ratio.

As these results base on the detected Raman-signals, which possibly penetrate the transformed zone as well as the tetragonal structure, further attention should be drawn to the signal depth. This is furthermore useful in order to correlate the description of the phase transformation behavior by MAJ law to the continuous progression of a completely transformed zone into the bulk material. A modified Lambert-Beer approach can be applied in order to determine the signal intensity $I_n(z)$ for a certain signal depth z and wave number n . As depicted in Equation 10, the signal intensity shows an absorbance at transmission through a finite material thickness expressed by a specific extinction constant $\alpha_{n,mono-tetr}(z)$.

$$\Delta I_n(z) = -I_n(z) \cdot \alpha_{n,mono-tetr}(z) \cdot \Delta z \quad \text{Equation 10}$$

The exponential decay of the Lambert-Beer law is attained by integration from $z = 0$ to $z = Z$. But for the integration of the extinction of each signal, $\alpha_{n,mono-tetr}(z)$ has to be used for each wavenumber in consideration of the different microstructures. The intensity I_n of the emitted, returning inelastic signal is assumed to be proportional to the intensity of the primary signal I_0 for each wave number by Equation 11.

$$I_n(z) \propto I_0 \cdot e^{-\alpha_{n,mono-tetr}(z) \cdot z} \quad \text{Equation 11}$$

To calculate the returning signal at certain depth z , the extinction of the elastic signal into and the extinction of the inelastic signal out of the material can be numerically or analytically integrated, by using specific extinction constants.

Since a separation of the extinction for monoclinic and tetragonal microstructure seems to be sufficient for the recent progress, a mixing rule (Equation 12) was used to determine the extinction coefficient in dependence of the calculated intensity ratio V_m .

$$\alpha_{n,mono-tetr} = \alpha_{n,tetr} \cdot (1 - V_m) + \alpha_{n,mono} \cdot (V_m) \quad \text{Equation 12}$$

Since Raman signals were measured at the surface passing through the transformation zone as well as within cross-sectioned specimen, it was possible to compare the results and check the practicability of the Lambert-Beer behavior. The values for $\alpha_{n,mono}$ and $\alpha_{n,tetr}$ were determined by using a solver and minimization of the sum for all quadratic differences for the values of modeled and measured results. It was found, that a better adaption was achieved by using the same extinction constant, $\alpha_{n,mono} = \alpha_{n,tetr} = \alpha_n = 1/185 \mu\text{m}$, for the monoclinic and tetragonal material. On the one hand, it is assumed, that the extinction coefficients of the monoclinic and tetragonal phase shall be almost identical, as the materials' composition didn't change due to transformation. On the other hand, the data volume is not sufficient enough to adequately model the intensity ratio considering two different constants. As it can be seen from Fig. 10 the modelled intensity ratios match better to the optimal fit with the adaption of one extinction constant compared to the resolution with 2 constants. With $\alpha_{n,tetr} = 1/57 \mu\text{m}$ and $\alpha_{n,mono} = 1/708 \mu\text{m}$, the two constants are assessed to differ too much from each other to describe physically realistic values.

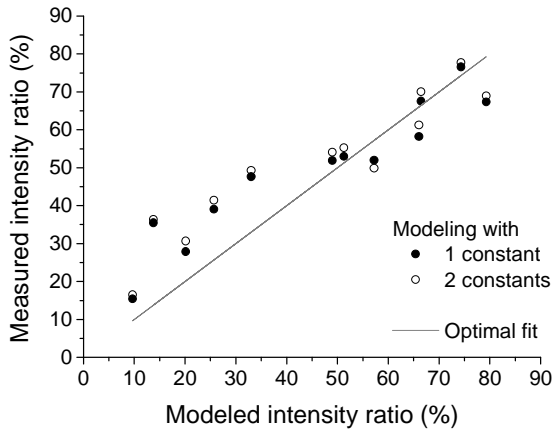


Fig. 10: Comparison of the modelled intensity ratios, which were calculated with 1 and 2 extinction constants, and the intensity ratios from Raman-spectroscopic measurements at the surface.

Thus, in the following only one extinction constant was used. With regard to the promising compliance, it was tested if the findings mathematically match the MAJ behavior for a growing transformation zone.

A further simplification was made by setting the intensity ratio $V_m(z) = 80\%$ within and $V_m(z) = 0\%$ outside of the transformation zone. The temperature-dependent growth rate m of the transformation zone determines the progression of its depth $d(t)$, as depicted in Fig. 4 and Equation 13.

$$d(t) = m \cdot t \quad \text{Equation 13}$$

The development of Raman intensities measured at the surface through the transformation zone with time can then be modelled as described in Equation 14. The prefactor 2 of this approach takes the return path of the laser light from the subsurface material to the detector into account.

$$V_m(t) = \frac{2\alpha}{I_0} \left(\int_0^{d(t)} V_m(z) \cdot I_0 \cdot e^{-2\alpha \cdot z} dz + \int_{d(t)}^z V_m(z) \cdot I_0 \cdot e^{-2\alpha \cdot z} dz \right) = 80\% \cdot (1 - e^{-2\alpha \cdot d(t)}) \quad \text{Equation 14}$$

This behavior is similar to the modified MAJ behavior with an Avrami-exponent $n = 1$, as depicted in Equation 9. Consequently, it is feasible to describe the extinction coefficient as relation of the reaction rate constant b and the rate of growth of the transformation zone m as described in Equation 15.

$$\alpha = \frac{b \cdot t}{2 \cdot d(t)} = \frac{b}{2 \cdot m} \quad \text{Equation 15}$$

Substituting the observed values for b and m for the investigated temperatures into Equation 15, leads to three values for the extinction coefficient:

$$T = 175 \text{ }^\circ\text{C} \Rightarrow \alpha = 0,005 \text{ } \mu\text{m},$$

$$T = 200 \text{ }^\circ\text{C} \Rightarrow \alpha = 0,0043 \text{ } \mu\text{m} \text{ and}$$

$$T = 225 \text{ }^\circ\text{C} \Rightarrow \alpha = 0,0062 \text{ } \mu\text{m}$$

The best agreement with the numerically calculated value $\alpha_n = 1/185 \text{ } \mu\text{m}$ was obtained for the samples that had been aged at a temperature of $175 \text{ }^\circ\text{C}$. The slight differences between the extinction coefficients might be explained by the simple approximations which have been applied previously, as normally, the extinction coefficients should not be affected by temperature and rate of growth of the transformation process. However, from these results it can be stated, that the results from Raman-spectroscopic measurements at the surface generally match with the results from analyzing the progression of the transformation front.

Finally, for very small degradation depths $d \ll 1/\alpha$, a linear correlation (Equation 16) can be used to estimate rates of growth.

$$\frac{V_m(t)}{80 \%} = 2\alpha \cdot d(t) \quad \text{Equation 16}$$

For lifetime-predictions of zirconia applications, the consideration of changed mechanical properties and the correlation with hydrothermal loading conditions is essential. As outlined above, LTD causes a transformation of surface and subsurface areas accompanied with mechanically weakened microstructure.

Focusing on the determined mechanical properties of the transformation zone, it was observed that hardness and Young's modulus are decreased. Previously [25] [26] [27], it was already found out, that these mechanical characteristics are significantly lower for monoclinic compared to tetragonal zirconia.

On the one hand, the weakened hardness is ascribed to the generation of twinning modes within the monoclinic phase [27]. On the other hand, the decrease of hardness and modulus are asserted to result from micro-cracks [26]. In summary, both twinning and micro-cracking influence the deformation behavior.

For the applied nanoindentations, twinning is supposed to affect the hardness and modulus decrease more significantly than micro-cracking. This conclusion is drawn from the findings illustrated in Fig. 8 which shows that the loading and unloading curves of the indentations within the monoclinic structure have a steady progression. In contrary, the curves are expected to scatter due to micro-cracking causing erratic pull-out and sliding of grains against each other. Still, it is supposed, that grain boundaries open respectively grains slide against each other due to tensile stresses in the far-field of the indentation.

However, the stiffness is not affected by micro-cracks as the calculated values for the monoclinic and tetragonal phase are observed to be almost equal. As generally a high presence of micro-cracks should decrease the stiffness [2], the weakening effect is apparently suppressed. This is assumed to result from compressive stresses which are expected to close cracks in the near-field beneath the indentation.

With regard to the structural integrity, it was however observed, that hydrothermal loading at 200 °C for 24 h and 225 °C for 8 h causes spontaneous fracture of the samples without any applied mechanical loading. These fractures due to LTD can be ascribed to internal stresses, which exceed the strength of the material as pointed out by Swain recently [28]. Therefore, the analysis of stresses which are generated by the progression of the transformation zone, considering the different Young's modules of zone and bulk material, calls attention to future work.

Hardness measurements that were applied subsequently to relatively intensive hydrothermal loading conditions may even lead to spalling at the edges of the indentation. This observation indicates decreased fracture toughness. In this regard, Fig. 11 shows exemplarily a Vickers indentation after hydrothermal loading for 8 h at 225 °C.

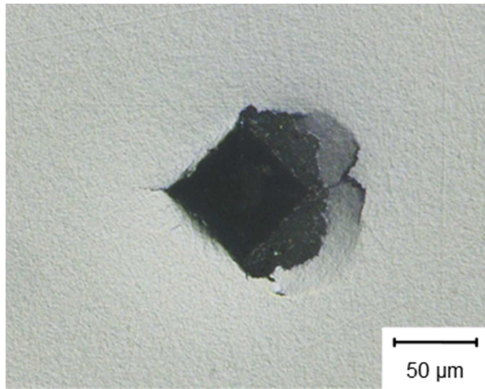


Fig. 11: Break-out of material after Vickers indentation with a loading force of 49 N and previous hydrothermal loading for 225 °C and 8 h.

Due to the asymmetric cracking from the corners and break-out at the edges, the determination of fracture toughness via Vickers indentation [29] is not suitable for hydrothermally loaded Y-TZP ceramics. Anyway, this method has to be used carefully since surface information about degraded zirconia cannot be assigned to bulk properties.

Fig. 7 shows an exponential decrease of macro-hardness with increasing transformation depth which results from changed mechanical properties in the transformation zone. However, it is supposed that the tetragonal subsurface areas below the indentation affect the hardness values and thus, the deeper the stable bulk material is located from the surface, the lower is its impact on the surface hardness. Therefore, the decrease of hardness reaches a saturation value at a particularly deep zone. With consideration of the observed spontaneous fracture, a total loss of cohesion can be expected for a completely LTD-transformed sample.

However, approximations of hardness values are acceptable within the measuring range and thus enable to ascribe changes of the material's mechanical response caused by the progression of the transformation front.

The Raman-spectroscopic and microscopic investigations of surfaces and cross-sections of hydrothermally loaded HY-TZP ceramics revealed a high resistance to hydrothermal degradation of this material. Consequently, the macro-hardness is not affected by exposure at various conditions in water steam atmospheres as the microstructure is not damaged by micro-cracks. Obviously, the

sintering process for HY-TZP results in a different and much more stable microstructure compared to Y-TZP. There are two features that discriminate the microstructure of HY-TZP and Y-TZP and which are responsible for the different transformation behaviors: first, the grain size of HY-TZP is significantly smaller in comparison to the standard Y-TZP. Due to the smaller grain size, the surface energy per unit volume increases. This energy is beside the chemical free energy and strain energy a part of the differential free energy of a unit volume which has to be applied to activate phase transformation [30]. Second, it can be assumed that the sintering increases the oxygen vacancy content, which is indicated by a light grey appearance of the HY-TZP material. Chevalier [3] stated that the overcrowding of oxygen around zirconium cations causes phase transformation. Hence, stabilization can be realized by incorporating oxygen vacancies into the microstructure by alloying yttrium. It is assumed that due to hydrothermal loading water-derived species like O^{2-} or OH^- fill these oxygen vacancies and thereby destabilize the tetragonal phase. Furthermore, the energy barrier for transformation is expected to decrease because of the consequently generated lattice distortions and micromechanical stresses. Therefore, a higher oxygen vacancy content is supposed to lead to a better stability of the tetragonal phase.

5 Conclusions

The results from measuring phase intensity ratios with Raman-spectroscopy at surfaces as well as cross-sections of hydrothermally loaded Y-TZP ceramics, the characterization of the progressing, hydrothermally induced transformation zones, the investigation of changed macro-hardness and the comparison with a HY-TZP ceramic lead to the following main conclusions:

- A sharp transition line separates the completely transformed zone and the tetragonal bulk material. The progression of phase transformation into the bulk material exhibits a time- and temperature-dependent, linear behavior. On the basis of these results and assuming constant hydrothermal loading conditions, the depth of the transformation zone as well as the rate of its growth can be described well for at least all conducted ageing experiments in the temperature range of 175 °C to 225 °C.
- Raman-spectroscopic measurements on the specimen surface reveal the often observed time- and temperature-dependent, exponential increase of the monoclinic phase intensity

ratio. However, these results do not represent the actual phase composition of the surface but are based on the superposition of transformed and not transformed signals that come from different material depths. Though, the measured intensity ratio can be used in combination with mechanical and microstructural characteristics to predict the consequences of LTD on the material.

- Furthermore, the results from Raman-spectroscopic measurements at the surface correlate with the progression of the transformation zone into the bulk material. By assuming one extinction coefficient for both tetragonal and monoclinic microstructure it is possible to calculate the depth of the transformation zone from the measured intensity ratio. The extinction coefficient can then be interpreted as relation of reaction rate constant and rate of growth.
- The mechanical properties determined via nanoindentation tests reveal a decreased hardness and Young's modulus of the transformation zone in comparison to the tetragonal structure. This decrease is supposed to result from twinning and micro-cracking within the transformation zone. However, the stiffness of both, transformation zone and tetragonal structure was observed to be almost equal. The macro-hardness of the zirconia ceramic decreases exponentially with increasing depth of the transformation zone due to the weakened microstructural integrity of this zone.
- HY-TZP shows a higher resistance to hydrothermally induced phase transformation than standard Y-TZP. Neither was phase transformation observed inside the material nor at the surfaces, thus the macro-hardness is not affected by hydrothermal exposure. As the composition is the same as for Y-TZP, the better resistance is explained by the smaller grain size and increased oxygen vacancy content.

6 Acknowledgements

The research project 16856 N of the research association "Forschungsgemeinschaft der Deutschen Keramischen Gesellschaft e. V." was financed within the program to promote the Industrial Joint Research (IGF) by the Federal Ministry for Economic Affairs and Energy (BMWi) via the German Federation of Industrial Research Associations (AiF) according to a decision of the German Federal Parliament. The authors address grateful acknowledgements for the financial support.

7 References

- [1] Manicone PF, Iommetti PR, Raffaelli L. An overview of zirconia ceramics: Basic properties and clinical applications. *J Dent* 2007;35:819-26
- [2] Basu B. Toughening of yttria-stabilised tetragonal zirconia ceramics. *Int Mater Rev* 2005;50:239-56.
- [3] Chevalier J, Gremillard L. The Tetragonal-Monoclinic Transformation in Zirconia: Lessons Learned and Future Trends. *J Am Ceram Soc* 2009;92:1901-20.
- [4] Hannink R, Kelly P, Muddle BC. Transformation Toughening in Zirconia-Containing Ceramics. *J Am Ceram Soc* 2000;83:461-87.
- [5] Rahaman MN, Yao A, Bal BS, Garino JP, Ries MD. Ceramics for Prosthetic Hip and Knee Joint Replacement. *J Am Ceram Soc* 2007;90:1965-88.
- [6] Chevalier J. What future for zirconia as a biomaterial? *Biomater* 2006;27:535-43.
- [7] Muñoz-Tabares JA, Jimenez-Pique E, Anglada M. Subsurface evaluation of hydrothermal degradation of zirconia. *Dent Mater* 2011;59:473-84.
- [8] Kelly JR, Denry I. Stabilized zirconia as a structural ceramic: An overview. *Dent Mater* 2008;24:289-98.
- [9] Schneider J, Begand S, Kriegel R, Kaps C, Glien W, Oberbach T. Low-Temperature Aging Behavior of Alumina-Toughened Zirconia. *J Am Ceram Soc* 2008;91:3613-8.
- [10] Chevalier J, Gremillard L, Deville S. Low-Temperature Degradation of Zirconia and Implications for Biomedical Implants. *Annu Rev Mater Res* 2007;37:1-32.
- [11] Das RS, Agrawal YK. Raman spectroscopy: Recent advancements, techniques and applications. *Vibrational Spectroscopy* 2011;57:163-76
- [12] Lughì V, Sergo V. Low temperature degradation -aging- of zirconia: A critical review of the relevant aspects in dentistry. *Dent Mater* 2010;26:807-20.
- [13] Gremillard L, Chevalier J, Epicier T, Deville S, Fantozzi G. Modeling the aging kinetics of zirconia ceramics. *J Eur Ceram Soc* 2004;24:3483-9.
- [14] Schneider J. Untersuchungen zum Alterungsverhalten und zur Langzeitstabilität von Y-TZP/Al₂O₃-Dispersionskeramiken (ATZ) für die Anwendung in der Hüft-Endoprothetik. PhD thesis, Weimar: Bauhaus University; 2012.
- [15] Presser V, Keuper M, Berthold C, Nickel KG. Experimental Determination of the Raman Sampling Depth in Zirconia Ceramics. *Appl Spectrosc* 2009;63:1288-92.
- [16] Keuper M, Eder K, Berthold C, Nickel KG. Direct evidence for continuous linear kinetics in the low-temperature degradation of Y-TZP. *Acta Biomater* 2013;9:4826-35.
- [17] DIN EN 843-4. Hochleistungskeramik - Mechanische Eigenschaften monolithischer Keramik bei

Raumtemperatur - Teil 4: Härteprüfung nach Vickers, Knoop und Rockwell. 2006.

- [18] Clarke DR, Adar F. Measurement of the Crystallographically Transformed Zone Produced by Fracture in Ceramics Containing Tetragonal Zirconia. *J Am Ceram Soc* 1982;65:284-8.
- [19] Dorn M. Phasenumwandlung in TZP-ZrO-Zirkonoxid durch lokale mechanische Belastung. PhD thesis, Tübingen: University of Tübingen; 2003.
- [20] Muñoz-Tabares JA, Anglada MJ. Quantitative Analysis of Monoclinic Phase in 3Y-TZP by Raman Spectroscopy. *J Am Ceram Soc* 2010;93:1795-5.
- [21] Oliver W, Pharr G. Measurement of hardness and elastic modulus by instrumented indentation: Advances in understanding and refinements to methodology. *J Mater Res* 2004;19:3-20.
- [22] Gaillard Y, Jiménez-Piqué E, Soldera F, Mücklich F, Anglada M. Quantification of hydrothermal degradation in zirconia by nanoindentation. *Acta Mater* 2008;56:4206-16.
- [23] Sakharova N, Fernandes J, Antunes J, Oliveira M. Comparison between Berkovich, Vickers and conical indentation tests: A three-dimensional numerical simulation study. *Inter J Sol Struct* 2009;46:1095-104.
- [24] Pezzotti G, Yamada K, Sakakura S, Pitto RP. Raman Spectroscopic Analysis of Advanced Ceramic Composite for Hip Prosthesis. *J Am Ceram Soc* 2008;91:1199-206.
- [25] Sakuma T, Yoshizawa YI, Suto H. The microstructure and mechanical properties of yttria-stabilized zirconia prepared by arc-melting. *J Mater Sci* 1985;20:2399-407.
- [26] Cutler RA, Reynolds JR, Jones A. Sintering and Characterization of Polycrystalline Monoclinic, Tetragonal, and Cubic Zirconia. *J Am Ceram Soc* 1992;75:2173-83.
- [27] Chen I-W. Implications of Transformation Plasticity in ZrO₂-Containing Ceramics: II, Elastic-Plastic Indentation. *J Am Ceram Soc* 1986;69:189-94.
- [28] Swain MV. Impact of oral fluids on dental ceramics: What is the clinical relevance?. *Dent Mater* 2014;30:33-42.
- [29] Anstis G, Chantikul P, Lawn BR, Marshall DB. A Critical Evaluation of Indentation Techniques for Measuring Fracture Toughness: I, Direct Crack Measurements. *J Am Ceram Soc* 1981;64:533-8.
- [30] Lange FF. Transformation toughening Part 1: Size effects associated with the thermodynamics of constrained transformations. *J Mater Sci* 1982,17:225-34.